J. Biomechanics Vol. 23, No. 8, pp. 823–836, 1990.
Printed in Great Britain

0021-9290/90 $3.00 + .00

PHYSICAL MODEL SIMULATIONS OF BRAIN INJURY IN THE PRIMATE

SUSAN SHEPS MARGULIES,*†‡ LAWRENCE E. THIBAULT* and THOMAS A. GENNARELLI§

* Department of Bioengineering, University of Pennsylvania, Philadelphia, PA 19104, U.S.A. and
§Department of Neurosurgery, University of Pennsylvania, Philadelphia, PA 19104, U.S.A.

Abstract—Diffuse brain injuries resulting from non-impact rotational acceleration are investigated with the aid of physical models of the skull–brain structure. These models provide a unique insight into the relationship between the kinematics of head motion and the associated deformation of the surrogate brain material. Human and baboon skulls filled with optically transparent surrogate brain tissue are subjected to lateral rotations like those shown to produce diffuse injury to the deep white matter in the brain of the baboon. High-speed cinematography captures the deformations of the grids embedded within the surrogate brain tissue during the applied load.

The overall deformation pattern is compared to the pathological portrait of diffuse brain injury as determined from animal studies and autopsy reports. Shear strain and pathology spatial distributions mirror each other. Load levels and resulting surrogate brain tissue deformations are related from one species to the other. Increased primate brain mass magnified the strain amplified without significantly altering the spatial distribution. An empirically-derived value for a critical shear strain associated with the onset of severe diffuse axonal injury in primates is determined, assuming constitutive similarity between baboon and human brain tissue. The primate skull physical model data and the critical shear strain associated with the threshold for severe diffuse axonal injury were used to scale data obtained from previous studies to man, and thus derive a diffuse axonal injury tolerance for rotational acceleration for humans.

INTRODUCTION

Diffuse axonal injury (DAI) presents immediately after injury as a prolonged state of 'coma'. Histological examination reveals diffuse tissue trauma throughout the cerebral hemispheres and brain stem, with tissue tears and axonal damage in the corpus callosum, brain stem, and deep white matter of the hemispheres (Adams *et al.*, 1982a, b; Lindenberg *et al.*, 1955; Peerless and Rewcastle, 1967; Stritch, 1956, 1961). DAI is believed to be a primary injury, occurring at the time of accident, and not secondary to any other form of brain damage (Adams *et al.*, 1982b). Therefore, the motion of the brain during the event should be related to the tissue injuries seen at autopsy.

Previously, we developed an experimental model for DAI in the subhuman primate that reproduced the pathophysiological condition exactly as in the human (Gennarelli *et al.*, 1982). These experiments defined the loading conditions of the head that produce this brain injury by varying the direction of angular acceleration along horizontal, sagittal, lateral and oblique (head turned 30° to the left and moving posterior–anterior) planes. In each case, the head moved approximately 60°, the center of rotation remained at the C7/T1 vertebral level (with the exception of horizontal plane rotations where the center was at the brain's center of mass), and the magnitude of each acceleration was approximately the same. The incidence of traumatic unconsciousness with prolonged coma was greatest in purely lateral (i.e. coronal) plane accelerations (Gennarelli *et al.*, 1982, 1987).

It is technically difficult to measure the deformations within the brain of the animal model under the experimental conditions previously described. Alternatively, we have constructed physical models of the baboon skull/brain structure that are optically transparent and permit measurement of the distortions within the surrogate brain. We demonstrate that the magnitude and topographical distribution of the deformations within the surrogate brain during applied loads identical to those that produced DAI in the animal model correlate with the pathology in the animal experiments. Human skull physical models were subjected to lateral rotational accelerations of varying magnitude in order to determine the loading conditions that produce similar surrogate brain deformations. The physical modelling approach also lends insight into the study of brain injury tolerance. As an inanimate empirical scaling technique, physical models facilitate the prediction of human threshold for injury based upon the results of animal research by providing a means for scaling information from one species to another.

MATERIALS AND METHODS

Skull physical models were constructed with materials and methods similar to those previously described (Margulies, 1987; Margulies *et al.*, 1985). Only specific

Received in final form 28 *December* 1989.
† Present address: Desk S-3 Plummer Bldg, Mayo Clinic, Rochester, MN 55905, U.S.A.
‡ To whom correspondence should be addressed.

steps that distinguish this series from previous physical model series will be discussed in detail.

Three models were constructed: two adult baboon (*Papio nubis*) skulls, one without a falx cerebri present (model B1) and one with a surrogate falx (model B2), and one adult human skull with a falx (model A1) (skulls from Carolina Biological Supply Co.).

The coronal plane passing through the pons, third ventricle, thalamus, and corpus callosum, just anterior to the auditory canal, contains the cerebral structures most frequently associated with diffuse neural tissue damage (Adams *et al.*, 1982a; Grcevic, 1982), and is the plane of interest in this study. A coronal cut was made in each skull approximately 1.5 cm posterior to the plane of interest. The anterior portion of each skull was used for the physical model and the posterior portion for the model counterweight. The counterweight balanced the kinematic linkage of the accelerating device (HYGE™ linear actuator, Bendix Corp.) during the applied loads, and was constructed in a similar fashion to the models. In addition, the anterior half of models B2 and A1 were also cut down the sagittal mid-line to allow for insertion of a surrogate falx.

The falx cerebri can be modelled as thin plate or membrane that is rigidly attached to the skull along its superior periphery, and free to move on the inferior edge. Life-size falxes for an adult human (Nieuwenhuys *et al.*, 1978) and baboon (Davis and Huffman, 1968) were cut from polyurethane (0.015" (381 μm) thickness for the baboon model B2 and 0.020" (508 μm) thickness for the human model A1), positioned along the sagittal midline cut of the appropriate model, and secured with epoxy between the two sagittal skull halves (Fig. 1). Polyurethane (MP1880, Stevens Elastomerics) was used because the ratio between its Young's modulus and that of the surrogate brain material (9000–20,000) is similar to the ratio between primate falx cerebri and brain tissue (7000–48,000) (Margulies, 1987). The inner surfaces of the skulls were painted white (Testor's Enamel, No. 1168) to enhance photographic resolution.

The foramen magnum in each model was covered, allowing no radial displacement at this boundary. As such, these models are not suitable for the investigation of certain brainstem injuries or injuries due to the herniation of the brain through the foramen magnum.

An open-ended cylindrical shell was constructed for each model from aluminum tube stock, and the bottom end machined to fit onto the kinematic linkage of the HYGE™ machine. The skull was positioned in the shell and secured in place with Castolite Resin (Buehler, Ltd) potting material such that the posterior surface of the skull was recessed slightly from the top edge of the shell. To prevent the Castolite from slipping against the smooth aluminum shell, 6 holes were drilled and tapped radially around the circumference of the shell about half-way up the height of the model, and screws were inserted into the Castolite. A layer of RTV Silicone Rubber (No. 108, General Electric) over the exposed Castolite assured a watertight seal on the bottom of the model.

To establish a 'brain weight' for the models, the weight of the gel used in the models must be determined. At this point in the construction, the potted anterior and posterior skull portions were weighed and these values were used as tare weights for the models. Later, the tare weight was subtracted from the final weight to calculate the 'brain' weight for each model.

The optically transparent surrogate brain material (silicone gel system, Dow Corning), mixed in a 1:1 ratio of polymer to catalyst, was poured into the skulls to the plane of interest. The gel material adhered readily to the skull surface, and to subsequent layers of gel. After curing, black enamel orthogonal grids were painted onto the surface of the gel in each model. As per previous physical models constructed in our laboratory, model B1 was painted with a 3 mm grid spacing.

To obtain higher resolution of strain and displacement in regions near the falx, Models A1 and B2 were painted with a 1.5 mm grid spacing in the central third of the model, and a 3 mm grid spacing elsewhere (Fig. 2).

A second layer of gel was poured into all three models, bringing this last layer flush with the cut surface of the skull. After curing, the models and posterior skull portions were weighed and total 'brain' masses calculated. The mass of the gel and the equivalent brain tissue mass respectively were 130 and 145 g for models B1 and B2, and 956 and 1067 g for model A1. The brain tissue mass was calculated by multiplying the gel mass by ρ_{brain}/ρ_{gel}, where $\rho_{brain} = 1.06$ g cm^{-3} and $\rho_{gel} = 0.95$ g cm^{-3}.

The falx in models A1 and B2 was firmly attached to the coverplate to simulate the strong attachment of the falx to the tentorium and occiput of the skull. In all the models, the gap between the gel surface and coverplate was filled with water to create a pure slip condition at that boundary, and the models were sealed with bone wax (Ethicon, Inc.) and RTV sealant.

The experimental system used to provide the loading conditions for the physical models was the same as that used in the animal model (Gennarelli *et al.*, 1982, 1987). The system consists of a 15.2 cm HYGE™ (Bendix) actuator and a kinematic linkage capable of delivering a well-distributed, impulsive load. Each model was mounted on the linkage of the HYGE™ with its counterweight on the opposite sidearm, and accelerated through a 65° arc with a biphasic, noncentroidal rotational load with a distance of 7.3 cm from the center of rotation to the center of mass of the model (see Fig. 3). The rigid-body tangential acceleration–time history of the shell was recorded using a piezoelectric accelerometer/charge amplifier/digit recording system (Endevco).

Deformations of the grid within the gel were filmed with a high-speed movie camera (HYCAM, Redlake Corp.) at 6600 frames per second. The timing of the

Fig. 1. Physical model construction. Baboon and human skull models with surrogate falx inserted in the midsagittal plane. This photograph was taken before the skulls were potted in their aluminum shells and then filled with the transparent gel material.

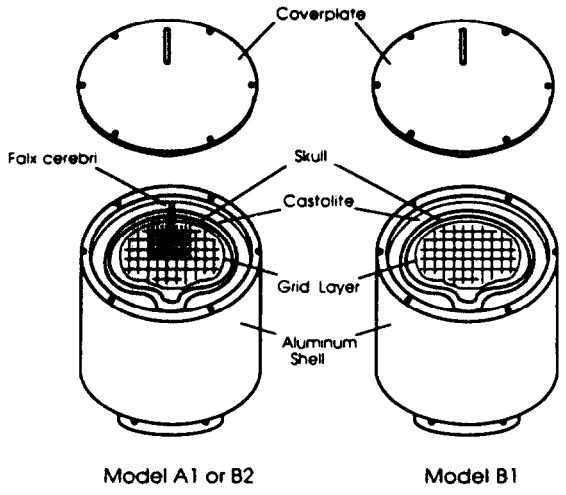

Fig. 2. Skull physical model schematic. On the left, a model with a falx cerebri in place and a finer grid painted in regions at high risk to tissue injury. On the right, a skull model with no falx cerebri.

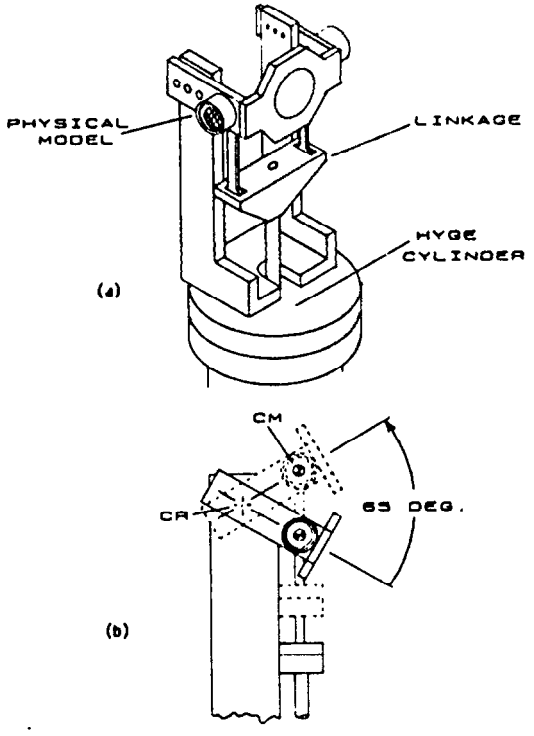

Fig. 3. Physical model mounted on HYGE™ accelerating system. (a) Kinematic linkage schematic. (b) Side view of linkage motion with 7.3 cm between model center of mass (CM) and center of rotation (CR).

lights, camera, and HYGE™ triggering was controlled by a custom-designed programmer-sequencer. Individual frames at 0.6 ms intervals were enlarged to life size and printed, and the grid deformations were digitized and stored in a Hewlett Packard 9836 computer. The rigid body motion of the shell/skull was subtracted out during the digitizing process, leaving behind only the relative motion of the gel with respect to the skull. The position of each node point, or grid intersection, was defined with 0.4 mm (0.017") resolution. At each node in the grid, Lagrangian angular displacement V was determined, and infinitesimal shear strain ε was calculated from the relationship

$$\varepsilon = \frac{1}{2}(\gamma_0 - \gamma) \quad (1)$$

where γ_0 is the angle formed by two adjacent line segments which intersect at the node of interest in the undeformed grid, and γ is the angle between the same two line segments in the deformed grid. A circle was fit to the cut edge of the skull in a printed frame from each experiment and the origin of the grid coordinate system for that experiment was defined as the center of this circle. The non-dimensional radial location of a node was defined as the node-to-origin distance divided by the radius of the circle.

Because the gel material properties varied slightly from model to model, the displacement and strain responses were normalized with respect to primate brain (E_{brain} = 30.77 cm H_2O or 0.437 psi) (Margulies, 1987; Blum, 1983). The normalizing factor, $Z_{modulus}$, was defined as

$$Z_{modulus} = E_{model}/E_{brain}.$$

Normalized displacements and strains were obtained by multiplying the unscaled response by $Z_{modulus}$. $Z_{modulus}$ for models B1, B2 and A1 were 1.65, 0.73, and 0.64 respectively.

EXPERIMENTAL PROTOCOL

The baboon skull physical model (B2) was accelerated in precisely the same manner and at similar load levels as previous animal studies to compare the intracranial deformations in the model with actual DAI lesion distributions in the baboon. The same HYGE™ acceleration and deceleration metering pins, kinematic linkage, experimental sequencer, and digital accelerometer package were used for both animal and physical model experiments.

To determine the appropriate load levels for baboon physical model B2, all cases of baboon (*Papio nubis*) which were accelerated in the lateral direction (coronal plane) with a noncentroidal rotation and resulted in concussion or DAI were selected from the animal data. The available pathology information was gathered for each of 52 cases of DAI and nine cases of concussion, and the duration τ_D and peak rotational acceleration $\ddot{\theta}_p$ were calculated for the acceleration and deceleration phases of the applied load. A triangular decleration pulse shape was assumed for the calculations of peak change in angular velocity $\Delta\dot{\theta}_p$ ($\Delta\dot{\theta}_p = 0.5 \times \ddot{\theta}_p \times \tau_D$). Brain mass was recorded when available; some experimental protocols did not allow for the brain to be weighed and an average baboon brain mass of 140 g was assumed.

The peak deceleration and angular velocity data were scaled to the brain tissue mass of model B2

(145 g) using Holbourn's scaling relationship (Holbourn, 1956; Ommaya *et al.*, 1967):

$$\ddot{\theta}_{B2} = \ddot{\theta}_{Baboon}\left(\frac{M_{Baboon}}{M_{B2}}\right)^{2/3} \quad (2)$$

$$\dot{\theta}_{B2} = \dot{\theta}_{Baboon}\left(\frac{M_{Baboon}}{M_{B2}}\right)^{1/3} \quad (3)$$

where

M_{Baboon} = brain mass of baboon

M_{B2} = 145 g, brain mass of B2

$\ddot{\theta}_p$ = rotational acceleration

$\dot{\theta}_p$ = rotational velocity.

Figure 4 illustrates the acceleration and velocity data scaled to the 145 g brain mass of model B2.

The data was clustered along a line due to the relatively fixed relationship between peak angular deceleration and pulse duration for a particular HYGE™ deceleration metering pin. Acceleration or deceleration magnitude and pulse duration (as well as pulse shape) can be varied independently by changing appropriate metering pins. Using the same metering pin combination in the animal model and physical model experiments reduced the number of degrees of freedom in the load configuration and permitted the use of the magnitude of the peak angular deceleration as the single independent applied load variable.

The animal study was designed to investigate severe DAI, and did not explore concussion and mild DAI thoroughly. An injury threshold for mild DAI would most likely be lower than the injury threshold derived from this animal data set.

In general, DAI occurred at higher levels of angular acceleration than concussion. Derived from animal data, the threshold for DAI in a baboon with a 145 g brain can be drawn at $\ddot{\theta}_p \approx 9.75 \times 10^4$ rad s^{-2}. When accelerated at or above this threshold, nearly all of the animals were diagnosed as having classic DAI, as seen in humans.

Model B2 was accelerated at five levels, ranging from mild concussion [dashed line in Fig. 4; determined from (Ommaya *et al.*, 1967) rhesus monkey data and scaled using equation (2)] to severe DAI. Four of these levels were scaled from a 145 g brain mass to the 1067 g brain mass of model A1 using equation (2). Model A1 was accelerated at these four levels, as well as at a level slightly below the DAI threshold estimate. Model B1, the baboon model without a falx, was accelerated at a concussive level identical to one used for model B2. All acceleration data appear in Table 1.

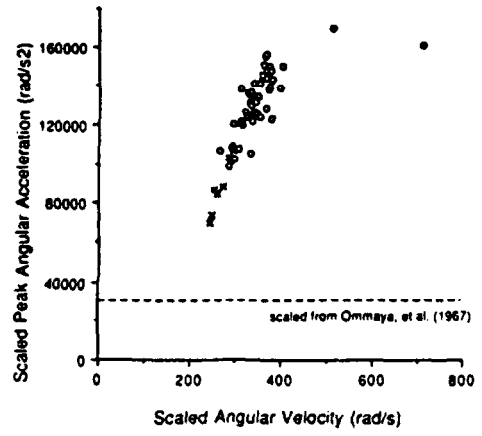

Fig. 4. Animal data for DAI and concussion. The subhuman primate data for DAI (○) and concussion (×), and the threshold for concussion proposed by Ommaya *et al.* (1967; dashed line) were scaled to 145 g brain mass using the relationship suggested by Holbourn (1956) and given by equations (2) and (3).

RESULTS

The influence of the falx cerebri on intracranial motion and deformation was investigated using the two baboon skull physical models. Otherwise nearly identical, model B1 was constructed without a falx, while a polyurethane falx was inserted with proper anatomical positioning in model B2.

Tethered at the skull and coverplate, the falx is a stiff fin extending in towards the center of the model. For small disturbances in the gel, accompanied by low

Table 1. Skull physical model applied load data

Run	Model	Acceleration phase $\ddot{\theta}_p$ (rad s^{-2})	Acceleration phase τ_D (ms)	Deceleration phase $\ddot{\theta}_p$ (rad s^{-2})	Deceleration phase τ_D (ms)
1	B1-100	2.32×10^4	8.4	4.14×10^4	9.2
2	B2-65	1.75×10^4	10.7	3.10×10^4	9.5
3	B2-100	2.63×10^4	9.2	4.69×10^4	8.2
4	B2-215	5.22×10^4	7.1	1.04×10^5	5.7
5	B2-265	5.91×10^4	6.5	1.21×10^5	5.4
6	B2-325	6.96×10^4	6.3	1.58×10^5	5.5
7	A1-18	0.37×10^4	20.2	0.76×10^4	21.4
8	A1-45	0.97×10^4	12.6	2.12×10^4	12.8
9	A1-55	1.20×10^4	12.2	2.51×10^4	11.6
10	A1-70	1.54×10^4	11.3	3.11×10^4	10.9
11	A1-90	1.77×10^4	10.3	3.89×10^4	10.9

stresses, the falx acts as a rigid barrier, changing the geometry of the mid-coronal plane and reducing the strains as a result of partitioning the gel.

Models B1 and B2 were accelerated at similar concussive levels of angular acceleration (Runs 1 and 3 in Table 1). Several digitized frames are reconstructed from each experiment in Figs 5 and 6. The peak deformation occurs at $t = 6.6$ and 15 ms for acceleration and deceleration phases, respectively. The inclusion of a falx reduces the intracranial deformations without drastically affecting the temporal aspect of the field parameters.

Three locations in model B1, and comparable regions in model B2, were selected to represent high-risk regions for tissue injury in DAI (see Fig. 7). Normalized shear strains were calculated in each model at all three locations (Fig. 8). The strains in Regions 1 and 2 are greatly reduced with a falx present. The strains in Region 3 are small, and are not significantly changed with the addition of the falx. Region 3, representing the corpus callosum, lies near the center of mass of the model. If the non-centroidal rotations of the head can be approximated by a pure rotational motion with the center of rotation coincident with the center of mass of the brain (Margulies and Thibault, 1989), we would expect that for low-level applied loads, any points at or near the center of mass would be contained in a relatively non-deforming region undergoing rigid body motion. As such, it is fortunate that this critical region of the brain is located in a naturally safe site.

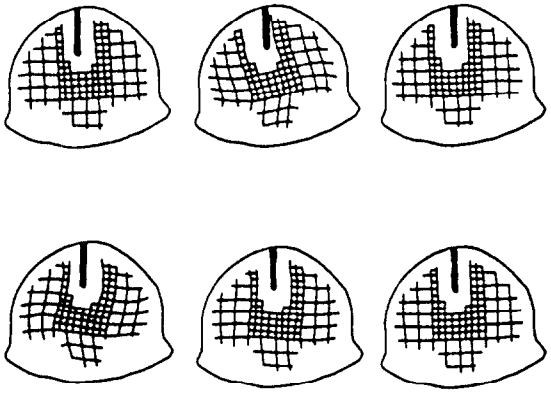

Fig. 5. Deformations of baboon model with falx cerebri. Reconstructed frames from model B2, Run 3, Table 1 at (from left to right beginning with the top row) $t = 0$, 6.6, 10.2, 15, 17.4, and 22.2 ms. The models in Figs 5 and 6 were accelerated with nearly identical applied loads. Deformation of the surrogate brain is reduced with falx cerebri present.

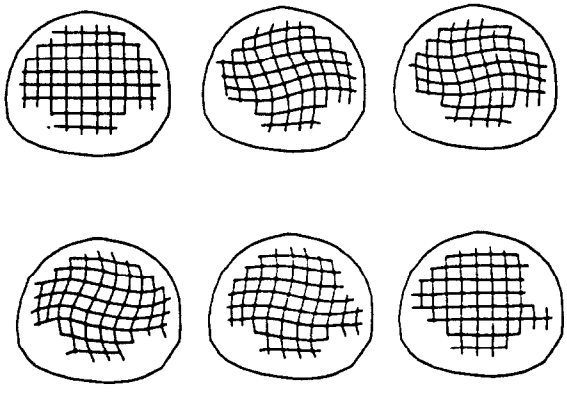

Fig. 6. Deformations of baboon model without falx cerebri. Reconstructed frames from model B1, Run 1, Table 1 at (from left to right beginning with the top row) $t = 0$, 6.6, 10.8, 15, 19.2, and 23.4 ms. See Fig. 5 caption.

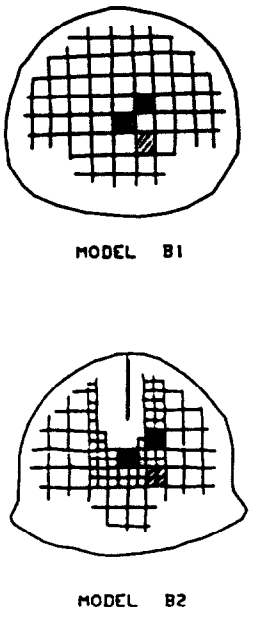

Fig 7. Regions studied to compare response of models B1 and B2. Region 1: shaded, top right; Region 2: cross-hatched, bottom right; Region 3: double cross-hatched, center left.

Figure 9a displays several computer-reconstructed digitized frames from a DAI-level experiment with model B2 (Run 5 in Table 1, $\ddot{\theta}_p = 1.21 \times 10^5$ rad s^{-2}). Some portions of the grid were obscured during the experiment due to technical difficulties with bone wax, glare, or air bubbles.

Those animals in Fig. 4 that were accelerated at roughly ($\pm 15\%$) the same magnitude as Run 5 in Table 1, and had neuropathological examinations (performed at the University of Glasgow), were selected. The post-injury survival time of the six animals selected varied from 1/2 h to seven weeks (median = 4.5 h). The gross and microscopic pathology reports from these animals were compiled, and Fig. 9b presents a composite of the lesion pathology in a mid-coronal plane similar to the plane of interest in model B2.

All brains were normal in size when excised, with no evidence of brain swelling. Small smears of blood were occasionally found in the subarachnoid or subdural spaces, especially near the site of the intracranial pressure monitoring bolt. 'Gliding contusions', tears in the brain tissue at the grey/white matter interface,

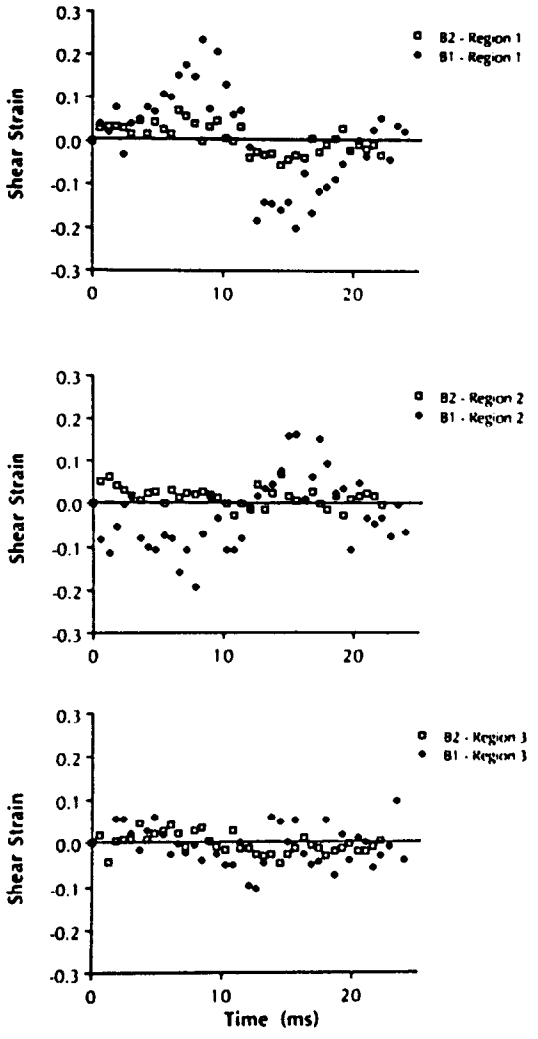

Fig. 8. Influence of falx cerebri on shear strain. Shear strains in models B1 (no falx) and B2 (falx) were normalized with respect to shear modulus (see text for details). The strains in Regions 1 and 2 are greatly reduced with a falx present. The strains in Region 3 are small, and not significantly changed with the addition of the falx.

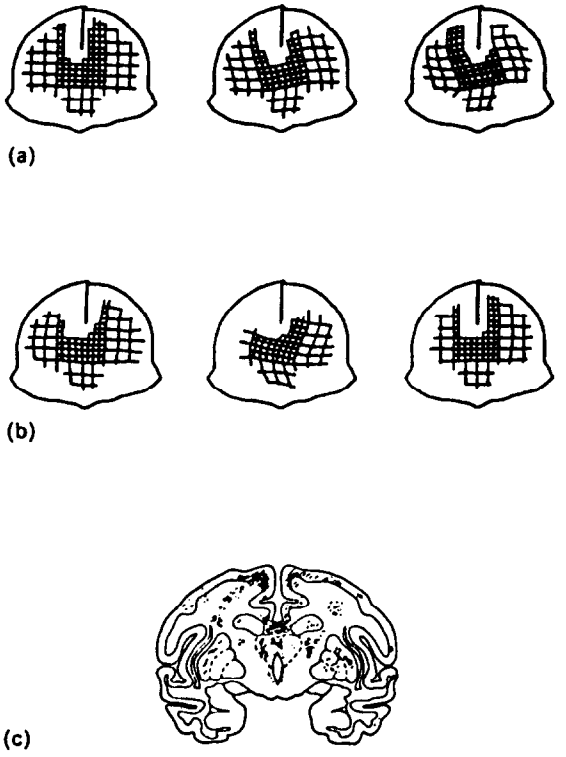

Fig. 9. Baboon skull model deformations in response to DAI-level load. Top: selected reconstructed digitized frames from model B2, Run 5, Table 1 at (from left to right beginning with the top row) $t = 0$, 3, 6, 7.8, 10.2, and 18.6 ms. Bottom: pathology composite of DAI in the baboon. Lesions occur most frequently in the medial third of the brain, which coincides with the region in the baboon skull physical model where deformations in the surrogate brain are largest in response to an applied load shown to produce DAI in the baboon.

were sometimes found in the superior parasagittal area near the falx. Focal lesions in the corpus callosum occurred frequently, and were usually located along the midline, extending to one side. Tissue tears were also found in the fornix, putamen, thalamus, and internal capsule. Often, axonal disruptions were found at sites of vascular injury (or hemorrhage). Diffuse axonal injury was identified throughout the white matter of the cerebral hemispheres in every case. Retraction balls were identifiable in the areas of damage, with very severe degeneration associated with the longest survival times.

Qualitatively comparing Figs 9a and 9b, the medial third of the brain is both the site of the largest number of lesions and the region in model B2 experiencing greatest deformation. Similarly, Fig. 10 presents a reconstruction of a DAI-level acceleration in model A1 (Run 9 in Table 1, $\ddot{\theta}_p = 2.51 \times 10^4$ rad s^{-2}). Once

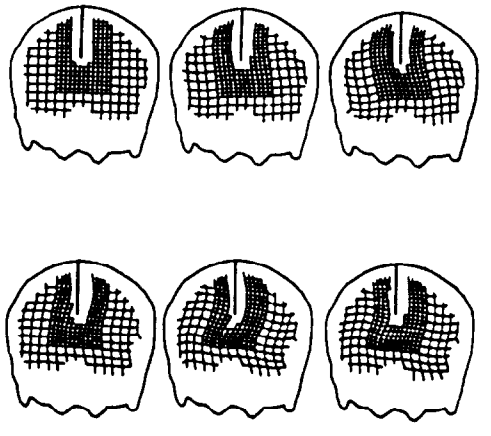

Fig. 10. Human skull model deformations in response to DAI-level load. Reconstructed digitized frames from model A1, Run 9, Table 1 at (from left to right beginning with the top row) $t = 0$, 3, 6, 12.6, 15.6, and 20.4 ms. The human and baboon (model B2, Fig. 9a) skull models show similar deformation patterns of the surrogate brain tissue when they are subjected to lateral rotational load levels which are predicted to produce DAI.

again, the region of the fine grid includes most of the large deformations. This 'large strain' region is coincident with the area that contains the highest incidence of injury in DAI. The grid in model A1 is distorted in the region of the corpus callosum, as well as the parasagittal area where gliding contusions occur. The models indicate that there is a direct relationship between deformation of surrogate brain tissue in physical models and tissue injury in animals.

Two sites were selected in Model B2 for analysis (refer to Fig. 11a); pathology data indicate that Region 1 is often injured in DAI, and Region 2 is injured less frequently. The position of the reference node point for each region was scaled to find the corresponding point in model A1 using the lateral and superior–inferior skull dimensions of the models (Fig. 11b).

The normalized shear strains were calculated in Region 1 of models B2 and A1 at 0.6 ms intervals (Table 1, Runs 2–5 and 7–10). For quantitative evaluation, a polynomial least-squares regression was performed on each data set. Theory and previous model results indicate that strain (ε) begins at a value of zero, returns to zero after the acceleration phase, deceleration phase, and after each oscillation in the acceleration-time history until the model comes to rest (Margulies and Thibault, 1989). The response followed a 3rd (and in some cases a 4th) order polynomial response of the form

$$\varepsilon = a_0 + a_1 t + a_2 t^2 + a_3 t^3 \ (+ a_4 t^4)$$

where t is time in ms. The term a_0 was set equal to zero, forcing strain to an initial value of zero.

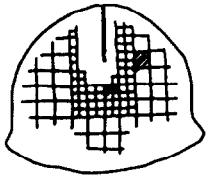

(a)

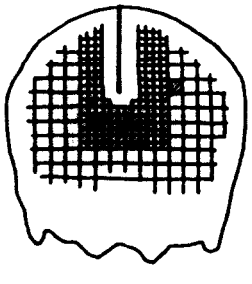

(b)

Fig. 11. Regions of interest in models B2 and A1. Region 1 (black rectangle, center) is at higher risk to injury than Region 2 (cross-hatched square, upper right). (a) Model B2; (b) Model A1.

The experimental data and corresponding polynomial models are plotted in Figs 12a–d and 13a–d, and the polynomial model coefficients and statistical information are presented in Table 2. Acceleration load values appear Table 1.

The quality of fit of the polynomial model to the data increases as the load level and magnitude of strain response increase. This trend is not surprising, for given fixed measurement errors (the combination of bit pad resolution and operator's ability to find the center of a grid crossing), proportional error in the strain calculation decreases as strain magnitude increases. Thus, for the lowest load level for model B2 (Fig. 12a) the deformations are quite small and near the limit of the resolution of the digitizing process. In model A1, even low-level accelerations produced strains large enough to minimize the effect of the scatter of the data. As a result, the quality of the fit of the polynomial models to the model A1 data was consistently higher than for model B2.

Figures 12 and 13 illustrate that for each experiment, strain begins at zero, takes on a maximum value around the time of peak acceleration, then crosses the x-axis to a minimum strain value during deceleration, and eventually returns to zero. ε_{max} is defined as the temporal maximum of the absolute value of shear strain, estimated from the polynomial representation of the strain response. Similarly, $\ddot{\theta}_p$ is defined as the absolute value of the largest rotational acceleration during the experiment. For the HYGE™ metering pin configuration used, $\ddot{\theta}_p$ always occurs at peak deceleration (refer to Table 1). With the exception of the B2-65 experiment where the mean of $\varepsilon = 0.0072$ represents the data as well as or better than the 3rd order polynomial model, ε_{max} occurred during the applied load's deceleration phase, shortly after $\ddot{\theta}_p$.

Figure 14 demonstrates that increasing rotational loads and model size results in increasingly higher strain levels; this finding is in agreement with earlier physical models with idealized geometry that were constructed in our laboratory (Margulies *et al.*, 1985). The experiment B2-215 (Run 4, Table 1), with a maximum rotational acceleration of 1.04×10^5 rad s^{-2}, most closely approximates threshold DAI in the baboon (refer to Fig. 4). This load level is defined as $\ddot{\theta}_{crit}$, the critical $\ddot{\theta}_p$ above which DAI is produced in a baboon (with a 145 g brain) accelerated in the coronal plane.

According to human and baboon pathology studies, Region 1 is the site of many of the hallmark lesions of DAI: tears in the corpus callosum, axonal damage (retraction balls, microglial scars, long tract degeneration), and petechial hemorrhages in the white matter (Adams *et al.*, 1982a, b; Grcevic, 1982; Peerless and Rewcastle, 1967; Stritch 1956, 1961). The level of strain in Region 1 of model B2, normalized to the shear modulus of baboon brain, is indicative of the strain present in the same location of a (145 g) baboon brain accelerated in the coronal plane at $\ddot{\theta}_{crit\text{-}B2}$. Assuming, as Holbourn did, that all primate brains have similar

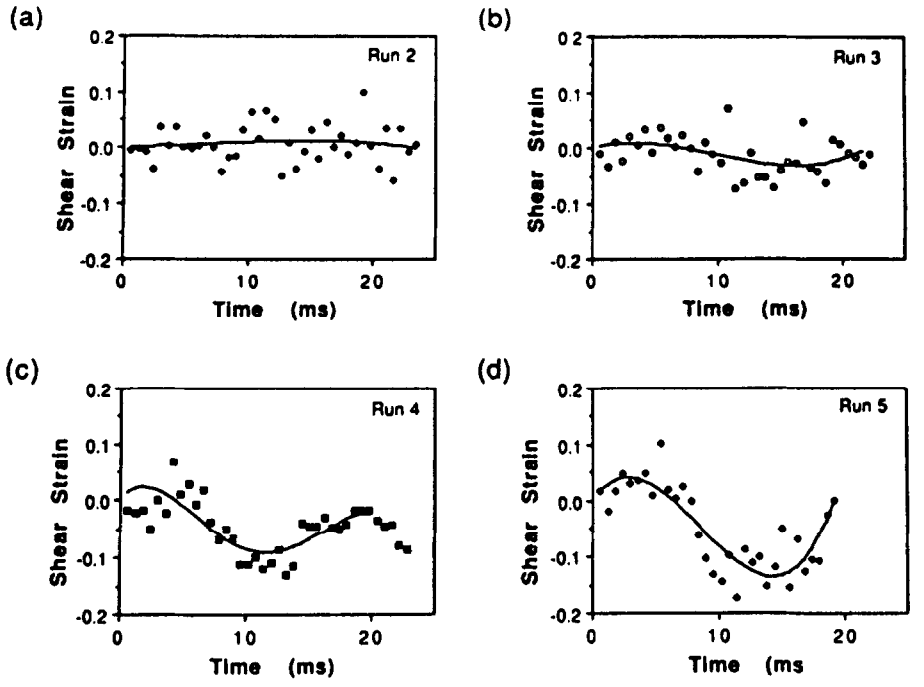

Fig. 12. Normalized shear strain time history—model B2, Region 1. Runs 2–5, Table 1. Shear strain was normalized with respect to shear modulus (see text for details). The 3rd or 4th order polynomial function fit to the data from each experiment is indicated by a solid line. Maximum shear strain magnitude (ε_{max}) occurs during the deceleration phase of the biphasic applied load. ε_{max} increases with increasing load magnitude.

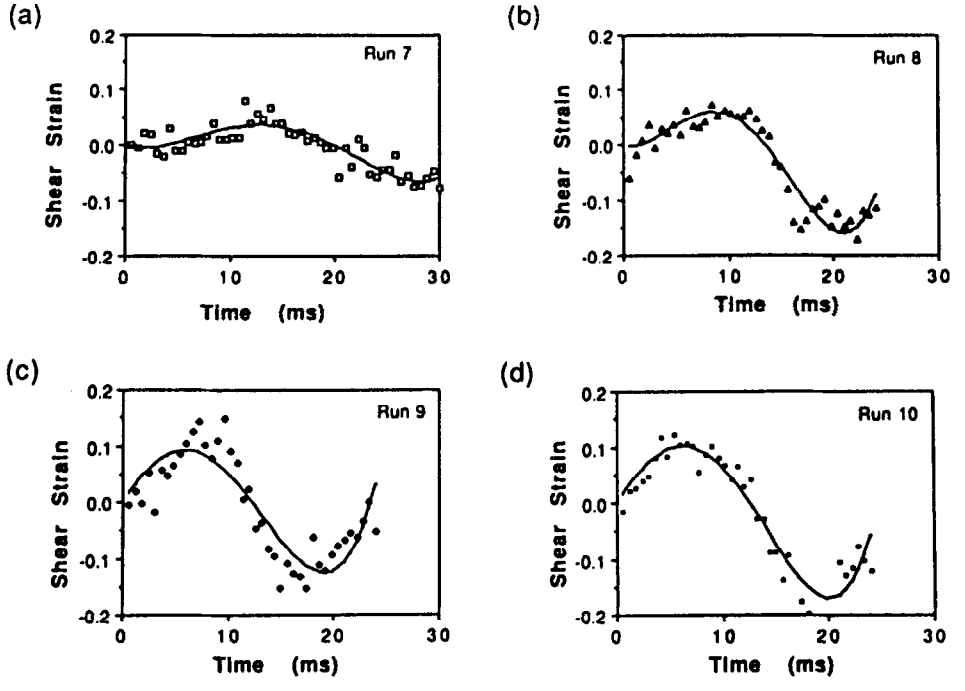

Fig. 13. Normalized shear strain time history—model A1, Region 1. Runs 7–10, Table 1. See Fig. 12 caption.

material properties and failure criteria for the neural and vascular components, the same strain at this particular location in other primate physical models would indicate similar tissue damage. Thus, injurious load levels can be scaled empirically from one species to another using skull physical models such as those discussed in this report.

To find equivalent harmful lateral rotational acceleration levels for the baboon and human we designate the level of strain in Region 1 at $\ddot{\theta}_{crit\text{-}B2}$ as $\varepsilon_{crit\text{-}DAI}$.

Table 2. Model B2 and A1 regression coefficients

Run	a_1	a_2	a_3	a_4	R^2
2	6.535E-4($P<0.9$)	8.472E-5($P<0.9$)	−4.870E-6($P<0.8$)	—	0.019
3	6.270E-3($P<0.12$)	−1.117E-3($P<0.05$)	−3.789E-5($P<0.04$)	—	0.180
4	2.667E-2($P<0.002$)	−8.631E-3($P<1E-4$)	6.606E-4($P<1E-4$)	−1.495E-5($P<1E-4$)	0.574
5	2.965E-2($P<1E-4$)	−6.169E-3($P<E-4$)	2.401E-4($P<1E-5$)	—	0.752
7	−6.102E-3($P<0.06$)	1.954E-3($P<0.002$)	−1.269E-4($P<4E-4$)	2.211E-6($P<4E-4$)	0.768
8	−6.940E-3($P<0.27$)	4.917E-3($P<0.002$)	−4.898E-4($P<1E-4$)	1.211E-5($P<1E-4$)	0.808
9	2.920E-2($P<0.005$)	−1.834E-3($P<0.6$)	−1.191E-4($P<0.6$)	6.126E-6($P<0.07$)	0.784
10	2.888E-2($P<6E-4$)	−1.212E-3($P<0.6$)	−1.785E-4($P<0.14$)	7.276E-6($P<0.01$)	0.909

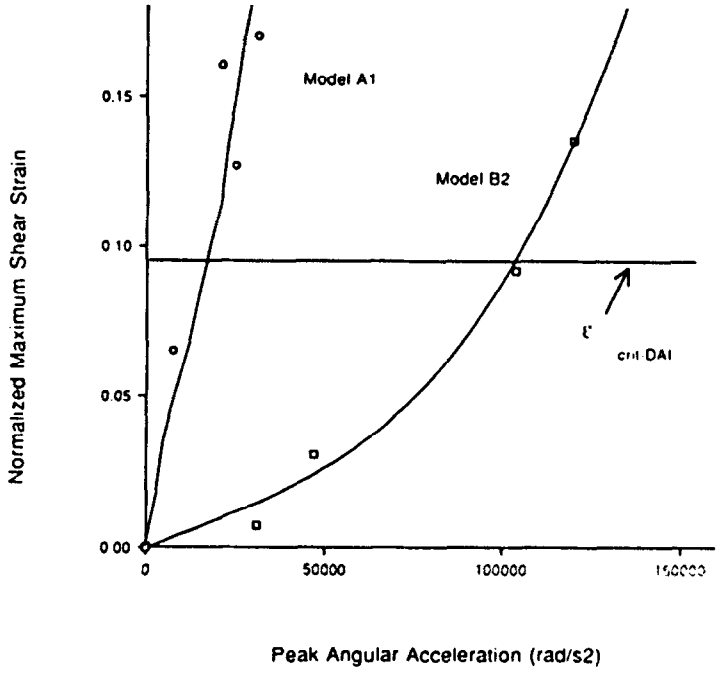

Fig. 14. Scaling threshold $\ddot{\theta}_p$ for DAI with skull physical models. ε_{max} increases with increasing model size and load level. The horizontal line indicates $\varepsilon_{crit\text{-}DAI}$, the shear strain threshold for DAI in Region 1 (Fig. 11) in the surrogate brain.

Combining experimental and physical model results, DAI exists when strain in this region is at or above $\varepsilon_{crit\text{-}DAI}$. Interpolating between the model B2 data in Fig. 14, $\varepsilon_{crit\text{-}DAI}$ is 0.094. $\varepsilon_{crit\text{-}DAI}$ is indicated with a horizontal line intersecting the model B2 data interpolation curve at $\ddot{\theta}_{crit\text{-}B2}$.

Assuming constitutive similarities between baboon and human brains, strains of $\varepsilon_{crit\text{-}DAI}$ or greater in Region 1 of model A1 indicate tissue injury characteristic of DAI. The intersection of the $\varepsilon_{crit\text{-}DAI}$ line with the model A1 data in Fig. 14 occurs at $\ddot{\theta}_{crit\text{-}A1}$, the coronal plane threshold acceleration for an adult human (with a 1067 g brain mass). Calculated from the interpolation line through the model A1 data, $\ddot{\theta}_{crit\text{-}A1}$ equals 1.60×10^4 rad s^{-2}. No lateral rotational data for humans is available in the literature to compare with these human physical skull model findings. In order to validate this tolerance level for man it would be useful to reconstruct accident scenarios that resulted in DAI and compare the data obtained from instrumented anthropomorphic dummies to the injury tolerance.

Region 2 in both models A1 and B2 is a location where human and baboon DAI pathology data indicated lesions occur much less frequently than in Region 1 (see Figs 9b and 11). Normalized shear strains and ε_{max} were calculated in this site as per Region 1. The relative displacement of Region 1 and Region 2 may have opposite signs as one moves ahead of the rigid body motion of the skull while the other point lags behind, producing strains of opposite sign. Therefore, considering the magnitude of the strains, $|\varepsilon_{max}|$, we find that $|\varepsilon_{max}|$ is greater in Region 1 than in Region 2 in both models. Assuming the two locations in the brain have similar material properties and failure criteria, smaller strains in Region 2 indicate less neural or vascular injury in that area, supporting the pathology evidence.

DISCUSSION

This paper presents a physical modelling method developed for the study of intracranial injury. Employing the physical models as an empirical scaling technique, we propose a rotational acceleration threshold for DAI in man. While acceleration itself does not produce brain injury directly, inertial loads are associated with a structural response of the brain that produces large strains, and presumably these strains are related to axonal pathophysiology present in DAI.

The major findings of the physical model experiments can be summarized as follows: firstly, the shear strain and brain tissue pathology spatial distributions mirrored each other, with highest strain levels in the physical models occurring in regions corresponding with those in the brain most often associated with DAI pathology. Thus, shear strain became an index for primary tissue injury due to rotational loads. Secondly, increased primate brain mass magnified the strain field without significantly changing its spatial distribution. Thirdly, by restricting the sideways motion of the hemispheres, the falx cerebri reduces intracranial dformations at lower load levels. Fourthly, the maximum strain levels (ε_{max}) in a region shown to be at high risk to axonal damage increased with maximum rotational acceleration ($\ddot{\theta}_p$) for both baboon and human brain sizes. Fifthly, and finally, threshold strain level was determined for this region of the baboon brain; strains at or above $\varepsilon_{crit\text{-}DAI}$ indicated the presence of DAI-type pathology. Assuming constitutive similarities between baboon and human brains, strains of $\varepsilon_{crit\text{-}DAI}$ or greater in the corresponding high-risk region of model A1 indicated tissue injury characteristic of DAI. The associated rotational acceleration threshold for a 1067 g human brain ($\ddot{\theta}_{crit\text{-}A1}$) was determined empirically.

The results presented in this report are in agreement with those of previous physical modelling efforts for general head injury. Early physical models created by Holbourn (1943, 1945) consisted of shear strain-sensitive gel poured into simplified wax models of the skull. He allowed the gel to partially adhere to the skull boundary and then applied sudden distributed rotational accelerations to the models while observing them through a circular polariscope. His results show that because brain tissue has a low shear modulus and relatively high bulk modulus (Stalnaker, 1969), the brain deforms most easily when the head is accelerated in a rotational manner. In addition, he found that the direction of the applied load and model geometry affected the strain pattern. More recently, Aldman *et al.* (1981) constructed physical models of idealized geometries ranging from cylinders to simplified skull forms, some with pure slip and others with no-slip allowed at the shell/surrogate brain boundary. They conducted a qualitative study demonstrating that skull geometry and skull/brain adhesion affect surrogate brain motion during rotational loads.

Because DAI has been shown to be a primary injury (Adams *et al.*, 1982b), this investigation focused on the distortions and injury of the brain that take place during a traumatic motion of the head. All pathology presented herein was acute in nature, occurring during the initial injury or immediately post-injury. The development of any subsequent pathology and, therefore, the long-term consequences of the traumatic incident, are complicated by a number of events which can occur sequentially or concurrently: hypoxia, ischemia in response to vascular injury, excitatory toxicity of the neurons, and receptor-mediated alteration in ion homeostasis. Depending on their severity and duration, these secondary events may have major or minor roles in predicting the long-term time course of a traumatic brain injury such as DAI.

There are several limitations of the physical models which deserve special mention: the skull geometry, the material properties of the surogate brain and falx, the representation of the skull/brain interaction, and the loading conditions. The skull geometry is accurate because real baboon and human skulls were used in the models, not idealized containers. Although the skull was cut to allow us to observe the motion of the gel, the free edge of the gel was lubricated to simulate the brain/brain interaction and to eliminate any influence of the Plexiglas coverplate on the distortions of the plane of interest, which was several cm below the free surface of the gel.

The material properties of the surrogate brain and falx materials undoubtedly influence the behavior of these structures. Indentation experiments with a small (O.D. = 1/16") rigid indentor were performed on the gel to determine the Young's modulus of each model (Margulies, 1987). Reported properties for brain tissue published in the literature vary by an order of magnitude (Thibault and Gennarelli, 1984). We found that the values of the gel vary by a factor of three within that range. To compare the deformations of different models, the data was normalized using the modulus of fresh brain (E_{brain} = 30.77 cm H_2O or 0.437 psi) which was determined using the same experimental indentation protocol and equipment (Blum, 1983). We determined the Young's modulus of baboon falx and candidate surrogate falx materials by clamping the membranes in a circular well and determining the relationship between the centerline displacement and the transmembrane pressure (Thibault and Fry, 1983; Margulies, 1987). We selected the urethane because the ratio between its Young's modulus and the gel was similar to the same ratio between primate falx and brain tissue.

The structural stiffness of the falx is due mainly to its rigid attachment along the superior margin to the skull. We represented that attachment at the skull by gluing the falx between the right and left halves of the models as seen in Fig. 1. At the free surface we tethered the surrogate falx firmly to the coverplate to simulate the strong attachment of the falx to the tentorium and

occiput. This rigid attachment is at the coverplate and not at the plane of interest with the grid. The free (inferior) edge of the falx at the plane of interest may have displaced as much as 3 mm in response to the larger loads, but this motion would have been obscured in the high-speed films because of the manner in which the falx was tethered to the coverplate.

The interaction between the skull and brain was represented by a no-slip boundary between the painted skull surface and the gel. The process of casting the gel in the skull leaves the gel firmly adhered to the inner surface of the skull. Previously, Margulies (1987) constructed two models of idealized geometry which were identical except that one had free slip and the other no slip on the shell/gel boundary. She compared the influence of the boundary constraint to that of skull geometry, and found that while pure slip reduced the distortion at the boundary and is perhaps a more accurate representation of the local interaction between brain and skull, the model geometry had more influence on the deformation of interior locations. The influence and import of a slip or no-slip interaction is attenuated quickly for locations more centrally located in the brain. Thus the skull models are limited to the study of the deep white matter where diffuse axonal injury is shown to occur.

The loading conditions used were limited in their range of acceleration magnitude and duration by the HYGE™ system. However, the loading device, acceleration and deceleration metering pins, duration and magnitude of the loads, and distance from the center of mass to center of rotation used in these physical model experiments were identical to those used in the baboon DAI experiments in Fig. 4. Thus there are no discrepancies in the applied loading conditions in the comparison between the deformations produced in the baboon physical model with the pathology distribution in actual baboons of the same brain size that underwent similar rotational accelerations.

It should be noted that the critical strain for DAI ($\varepsilon_{crit\text{-}DAI}$) represents a *local* strain threshold in the brain at a site often injured in cases of DAI. Because Gennarelli and Thibault (1982) and Gennarelli *et al.* (1987) found that DAI is produced more readily in coronal plane angular accelerations, only loads in this direction were considered. For accelerations oblique to the coronal plane, one might consider the coronal $\ddot{\theta}_p$ component of the load or the projection of the resultant acceleration vector onto the coronal plane. Also, it is important to emphasize that these threshold levels are derived from moderate to severe level DAI experiments and that thresholds for mild DAI would be lower.

To describe the phenomenon of DAI completely, one must develop similar local strain thresholds for rotational loads in other directions (e.g. sagittal and horizontal), perhaps using physical models constructed with appropriate planes of interest. In addition, varying degrees of inhomogeneity and anisotropy might be added to physical models where appropriate, resulting in even more life-like strain magnitudes and distributions in the models.

A physical modelling approach can be used in the study of other unique brain injuries. For example, acute subdural hematoma (ASDH), the traumatic and often fatal rupturing of the cerebral bridging veins, has been produced in the sub-human primate (Gennarelli and Thibault, 1982). Occurring as a result of rotational accelerations in the sagittal plane with very short time durations (typically <5 ms), ASDH could be studied with sagittal-section physical models. The region of interest in ASDH would be the cortical surface of the surrogate brain in a sub-human primate skull physical model. Together with isolated tissue studies of the bridging veins, an injury tolerance could be developed for ASDH.

Finally, physical models such as these would be useful for validating finite element or other types of analytical models designed to predict intracranial deformations.

Acknowledgements—Funds for this work were provided by NHTSA of the United States Department of Transportation, contract DTNH22-82-C07187.

REFERENCES

Adams, J., Gennarelli, T. and Graham, D. (1982a) Brain damage in non-missile head injury: observations in man and subhuman primates. In *Recent Advances in Neuropathology*, Ch. 7, pp. 165–190. Churchill Livingstone, New York.

Adams, J., Graham, D., Murray, L. and Scott, G. (1982b) Diffuse axonal injury due to non-missile head injury in humans: an analysis of 45 cases. *Ann. Neurol.* **12**, 557–563.

Aldman, B., Thorngren, L. and Ljung, C. (1981) Patterns of deformation in brain models under rotational motion. In *Head and Neck Injury Criteria—A Consensus Workshop*, pp. 163–168. U.S. Dept. of Transportation Publication DOT HS 806 434.

Blum, R. (1983) Dynamic indentation of the cerebral cortex (*in vivo*). Unpublished sr. design report, University of Pennsylvania, Philadelphia, PA.

Davis, R. and Huffman, R. (1968) *A Stereotaxic Atlas of the Brain of the Baboon*. University of Texas Press, Austin, TX.

Gennarelli, T. A. and Thibault, L. E. (1982) Biomechanics of acute subdural hematoma. *J. Trauma* **22**, 680–686.

Gennarelli, T. A., Thibault, L., Adams, J., Graham, D., Thompson, C. and Marcincin, R. (1982) Diffuse axonal injury and traumatic coma in the primate. *Ann. Neurol.* **12**, 564–574.

Gennarelli, T. A., Thibault, L., Tomei, G., Wiser, R., Graham, D. and Adams, J. (1987) Directional dependence of axonal brain injury due to centroidal and non-centroidal acceleration. *Proc. 31st Stapp Car Crash Conf.*, pp. 49–53. Society of Automotive Engineers, Warrendale, Philadelphia.

Grcevic, N. (1982) Topography and pathogenic mechanisms of lesions in 'inner cerebral trauma'. *Rad. Jazu. Med.* **4**, 165.

Holbourn, A. H. S. (1943) Mechanics of head injuries. *Lancet* **2**, 438–441.

Holbourn, A. H. S. (1945) Mechanics of brain injuries. *Br. Med. Bull.* **3**, 147–149.

Holbourn, A. H. S. (1956) Private communication to Dr Sabina Stritch, October 13, 1956.

Lindenberg, R., Fisher, R., Durlacher, S., Lovitt, W. and Freytag, E. (1955) Lesions of the corpus callosum following blunt mechanical trauma to the head. *Am. J. Path.* **31**, 297–317.

Margulies, S. S. (1987) Biomechanics of traumatic coma in the primate. Ph.D. dissertation, University of Pennsylvania, Philadelphia, PA.

Margulies, S. S. and Thibault, L. E. (1989) An analytical model of traumatic diffuse brain injury. *J. biomech. Engng* **11**, 241–249.

Margulies, S. S., Thibault, L. E. and Gennarelli, T. A. (1985) A study of scaling and head injury criteria using physical model experiments. *Proc. Int. Res. Council Biokinetics Impact*, pp. 223–234.

Nieuwenhuys, R., Voogd, J., Huijzen, C. van (1978) *The Human Central Nervous System: a Synopsis and Atlas*, p. 17. Springer, New York.

Ommaya, A. K., Yarnell, P., Hirsch, A. and Harris, E. (1967) Scaling of experimental data on cerebral concussion in sub-human primates to concussive thresholds for man. *Proc. 11th Stapp Car Crash Conf.*, pp. 73–80. Society of Automotive Engineers, Warrendale, Philadelphia, PA.

Peerless, S. J. and Rewcastle, N. B. (1967) Shear injuries of the brain. *Can. med. Ass. J.* **96**, 577–582.

Stalnaker, R. L. (1969) Mechanical properties of the head. Ph.D. dissertation, West Virginia University, Morgantown, VA.

Stritch, S. J. (1956) Diffuse degeneration of the cerebral white matter in severe dementia following head injury. *J. Neurol. Neurosurg. Psychiat.* **19**, 163–185.

Stritch, S. J. (1961) Shearing of nerve fibers as a cause of brain damage due to head injury. *Lancet* **2**, 443–448.

Thibault, L. E. and Fry, D. (1983) Mechanical characterization of membranelike biological tissue. *J. biomech. Engng* **105**, 31–38.

Thibault, L. E. and Gennarelli, T. A. (1984) Biomechanics and craniocerebral trauma. *Nervous System Status Report* (Edited by Povlishock, J. T.), Ch. 24, pp. 374–389. Public Health Services Press, Bethesda, MD.